


## Research Article

# Finite Element Model Updating of Satellite Sailboard Based on Sensitivity Analysis

Haitao Luo <sup>1,2</sup>, Wei Wang,<sup>3</sup> Jia Fu,<sup>1,2</sup> and Lichuang Jiao<sup>1,2</sup>

<sup>1</sup>State Key Laboratory of Robotics, Shenyang Institute of Automation, Chinese Academy of Sciences, Shenyang 110016, China

<sup>2</sup>Institutes for Robotics and Intelligent Manufacturing, Chinese Academy of Sciences, Shenyang 110016, China

<sup>3</sup>Institute of Mechanical Engineering and Automation, Northeastern University, Shenyang 110819, Liaoning, China

Correspondence should be addressed to Haitao Luo; [luohaitao@sia.cn](mailto:luohaitao@sia.cn)

Received 12 November 2018; Revised 10 February 2019; Accepted 20 February 2019; Published 21 March 2019

Academic Editor: Roger Serra

Copyright © 2019 Haitao Luo et al. This is an open access article distributed under the Creative Commons Attribution License, which permits unrestricted use, distribution, and reproduction in any medium, provided the original work is properly cited.

The modal analysis of a satellite sailboard finite element model is carried out to accurately investigate the response of a satellite sailboard in a complex loaded space environment through simulation. The basic excitation vibration test of the satellite sailboard is used to perform model matching and a correlation test. Appropriate design variables are selected through sensitivity analysis. Modal analysis data and vibration table excitation test response data are used to modify the finite element model. After optimization, the orthogonality of the simulated vibration mode and experimental vibration mode is good. The low-order frequency errors in the simulation model are less than 5%, the high-order errors are less than 10%, and the modal confidence MAC values are above 0.8. The modal frequency and mode shape are closer to the experimental modal frequency and mode shape, respectively. The simulation and test acceleration response of the modified finite element model of a honeycomb panel are compared under the two conditions of sine sweep and random vibration. The acceleration response curves of reference points are consistent, and amplitude and frequency errors are within acceptable limits. The model updating effect is evident, which provides good reference for research on satellites and other aerospace products.

## 1. Introduction

At present, a large number of composite materials are used in spacecraft products [1, 2]. Among them, honeycomb sandwich panels are widely used. They provide the advantages of high specific stiffness and specific strength and good heat insulation, vibration isolation, and impact resistance [3–7]. Honeycomb sandwich panel structures comprise 80–90% of the shell and shell structure of spacecraft [8, 9]. The simulation accuracy of its finite element model has an important impact on the environmental adaptability of rocket launch conditions (acceleration overload, vibration, impact, random noise, etc.). The dynamic parameters (modal matrix, coupling coefficient matrix,  $B_{\text{tran}}/B_{\text{rot}}$ , etc.) of the sailboard assembly of satellites provide a solid foundation for the precise control of the on-orbit attitude of satellites, as it is an extended large flexible accessory.

A satellite is subjected to an extremely harsh vibration shock and noise environment during use and launch. In particular, when a spacecraft launches and reenters the atmosphere at high speeds, the resulting random high-frequency vibrations and noise vibrations within the fairing can produce a mean square response acceleration of up to 50 g for the satellite structure. Therefore, it is necessary to carry out comprehensive dynamic analysis before launch to obtain accurate response prediction results for flight safety and good operation [10–12].

At present, the methods of satellite structural dynamics prediction are mainly the ground dynamics tests of structures, which are supplemented by finite element dynamics analysis. The vibration test of ground shakers is indispensable in the development and design of various types of satellites. Moreover, it is an important criterion for evaluating the conformity and safety of products [13, 14]. However, ground tests do not fully simulate the various environments and states

of a satellite during launch and on-orbit operation. In addition, the physical test period is long and expensive; this hinders the development of the satellite industry. The finite element simulation technology can conduct a comprehensive dynamic analysis of a product and obtain its response under various conditions. It is convenient to use, inexpensive, and has a short design period. Furthermore, it has become an important method of satellite product design and development and an important supplement to ground tests.

Finite element modelling consists of numerous theoretical assumptions, model simplification, distortion of connection conditions, and other factors. Additionally, satellite structures are extremely complex. Various components and auxiliary structures interact with each other, and different composite materials are widely used. For these reasons, it is quite difficult to establish an accurate and reasonable finite element model. There is error between finite element analysis results and experimental values. The dynamic response of models indicates that there is still a large gap between model results and actual situations. This strongly affects the reliability of finite element analysis. The design of satellite structures is bound to be highly conservative. The finite element model updating technology of satellite structures was proposed to solve this problem. An established finite element model was modified using a small amount of ground vibration test data. Then, the modified model was used for comprehensive dynamic response analysis to obtain reliable dynamic response prediction results.

In recent years, according to the method of resolving problems, a model updating method based on response surface analysis has been developed. This method transforms a finite element model updating problem from an inverse problem to a direct problem. Among numerous updating techniques, the design parametric model updating technique based on sensitivity analysis is the most mature.

The vibration mode correlation analysis between different models is an indispensable part of the model updating technology, and it can provide a basis for engineers to judge the quality of test analysis, the advantages and disadvantages of an initial finite element model, and sensor position optimization. For a certain order frequency, the degree of influence of each part of a structure is not the same. This is related to the mode distribution corresponding to the order frequency. If a certain part of a structure is in a region with large amplitude of a mode, then a slight change in this part will have a strong impact on the natural order frequency. On the contrary, if a part of a structure is close to the mode node, order frequency will not be significantly affected even if there is a large change in this part. In a project, it is expected that minor modifications to a structure will make its natural frequency meet requirements and will not affect the static strength and process requirements of the structure. In this study, the model of a solar panel is updated based on a correlation test and sensitivity analysis. A finite element model is obtained, which can accurately simulate the vibration response under complex aerospace conditions. This study provides a new idea for the precise finite element modelling of satellite solar panels and lays a strong foundation for the application research of satellite panels with realistic engineering significance.

## 2. Comparison of Modal Analysis and Modal Test of Satellite Sailboard

*2.1. Structure and Finite Element Modelling of Satellite Sailboard.* A regular hexagonal aluminum honeycomb sandwich panel with complex geometry is the most common form of honeycomb panel structures. Its geometry includes upper and lower panels, a central regular hexagonal honeycomb core, and a glue layer that connects the panels and a core layer. The glue layer is small in thickness and light in weight, and it is not the main bearing part. Therefore, the influence of the glue layer can be neglected in the analysis of honeycomb sandwich panels [15, 16]. The structure of a honeycomb sandwich panel is shown in Figure 1.

In Figure 1,  $a$  is the board length of the honeycomb sandwich panel;  $b$  is the board width;  $h_c$  is the thickness of the core; the thickness of the upper panel or lower panel is  $h_p$ ;  $t$  is the wall thickness of the core; and  $L$  is the length of the side.

The finite element model of a sailboard is established using PATRAN and NASTRAN (MSC Software Corporation). The model consists of upper and lower panels, a honeycomb core layer, a frame, a support base, and a compression sleeve. The upper and lower panels, frame, and intermediate cell are shell units, and the remaining are solid units. Adhesive connections are used between the parts. The expanded diagram of the model is shown in Figure 2.

The unit type and material properties of each part of the sailboard finite element model are provided in Table 1.

*2.2. Results of Modal Analysis and Test.* The constrained modal analysis of the established finite element model of the satellite sailboard is carried out. The modal frequency and mode shape of each order are obtained through modal analysis [17–22]. The simulation analysis of the mode shape of the finite element model of the satellite sailboard is shown in Figure 3.

The LMS test system is used to carry out a modal test on the satellite sailboard. The four corners of the sailboard are fixed on a fixture, and the fixture is fixedly connected with a vibration platform through bolts. Sixteen 4524-B acceleration sensors are uniformly distributed on the panel of the sailboard. A hammer drives the centre of the panel. A sensor port is connected to a cable for signal output, and the other end of the cable is connected with an acquisition system. The acquisition system outputs signals to a PC for data processing. The test setup is shown in Figure 4.

The arrangement of measurement sensors must be considered so that the final measurement result can easily reflect the vibration of the overall mode shape. Hence, the sensors should be arranged symmetrically and evenly on the entire satellite sailboard. The sensor arrangement in this test is shown in Figure 5. The sensors are placed at the ends and intersections of lines.

The various mode shapes of the test are obtained, and the first two mode shapes are shown in Figure 6.

*2.3. Model Matching and Correlation Test.* The correlation of the model includes frequency correlation and mode shape

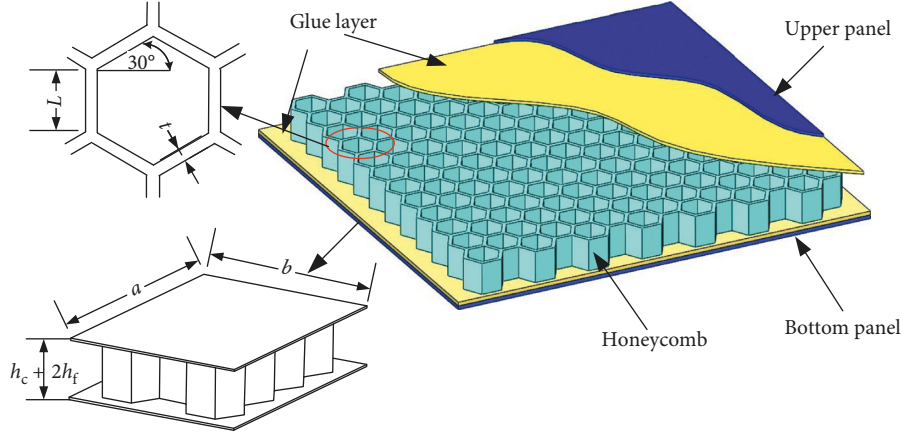


FIGURE 1: Honeycomb sandwich panel structure.

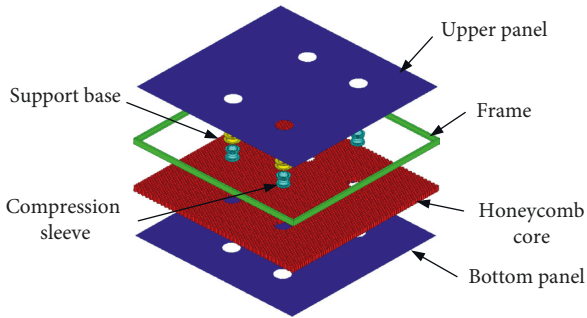


FIGURE 2: Expanded diagram of finite element model of sailboard.

TABLE 1: Unit type and material properties of each part of the sailboard finite element model.

| Component          | Unit type | Material        | Thickness attribute |
|--------------------|-----------|-----------------|---------------------|
| Panel              | CQUAD     | FRP             | 2 mm                |
| Honeycomb core     | CQUAD     | Aluminum alloy  | 0.02 mm             |
| Frame              | CQUAD     | Magnesium alloy | 0.5 mm              |
| Compression sleeve | CTETRA    | Titanium alloy  | —                   |
| Support base       | CTETRA    | Carbon fiber    | —                   |

correlation. Frequency correlation represents the degree of correlation between the modal test frequency ( $\omega_{EMA}$ ) and simulated analysis frequency ( $\omega_{FEA}$ ), and it is expressed as

$$\varepsilon\% = \frac{(\omega_{EMA} - \omega_{FEA})}{\omega_{FEA}}. \quad (1)$$

Ideally,  $\varepsilon$  should be close to zero. The larger the difference between  $\varepsilon$  and zero, the worse the correlation between  $\omega_{EMA}$  and  $\omega_{FEA}$  and vice versa.

Modal correlation indicates the degree of correlation between the mode shape of the modal test ( $\phi_{EMA}$ ) and that of the modal analysis ( $\phi_{FEA}$ ). Modal correlation is evaluated based on modal confidence (MAC), as shown in the following equation:

$$MAC_{EMA,FEA} = \frac{[\phi_{EMA}^T \cdot \phi_{FEA}]^2}{[\phi_{EMA}^T \cdot \phi_{EMA}] \cdot [\phi_{FEA}^T \cdot \phi_{FEA}]} \quad (2)$$

The MAC value is always between 0 and 1. If the value on the diagonal in the matrix is greater than or equal to 0.8, the simulation analysis mode has a good correlation with the corresponding experimental mode. In addition, if the values of the remaining positions in the matrix are less than or equal to 0.3, it implies that the modes corresponding to different orders have better independence and are not affected by each other. The computational logic block diagram of the correlation test is shown in Figure 7.

The first seven modal simulation results of the satellite sailboard are compared with the frequency and mode shapes of the test results. The obtained frequency values and mode shapes are inserted into the equations for frequency correlation (1) and mode shape correlation (2). The correlation of the models is calculated, and the results are shown in Table 2.

According to the correlation calculation results, the histogram for matching the MAC values of the simulation analysis mode and experimental mode is shown in Figure 8.

### 3. Sensitivity Analysis and Model Updating

**3.1. Introduction to Optimization Algorithm.** It has been proved that no single optimization algorithm can be applied to all structural optimization problems and a combined optimization strategy can achieve better results.

Here, the global search capability of an intelligent optimization algorithm (particle swarm optimization: PSO) [23, 24] and the local search capability based on a sensitivity analysis gradient method (NLPQL) are used to achieve a balance between optimization quality and optimization efficiency [25, 26].

An optimized Latin hypercube test is used to design sample points to prevent running the NASTRAN finite element program every time in the iterative process. The fourth-order polynomial response surface (RMS) model of structural response is constructed for further improving the optimization efficiency.

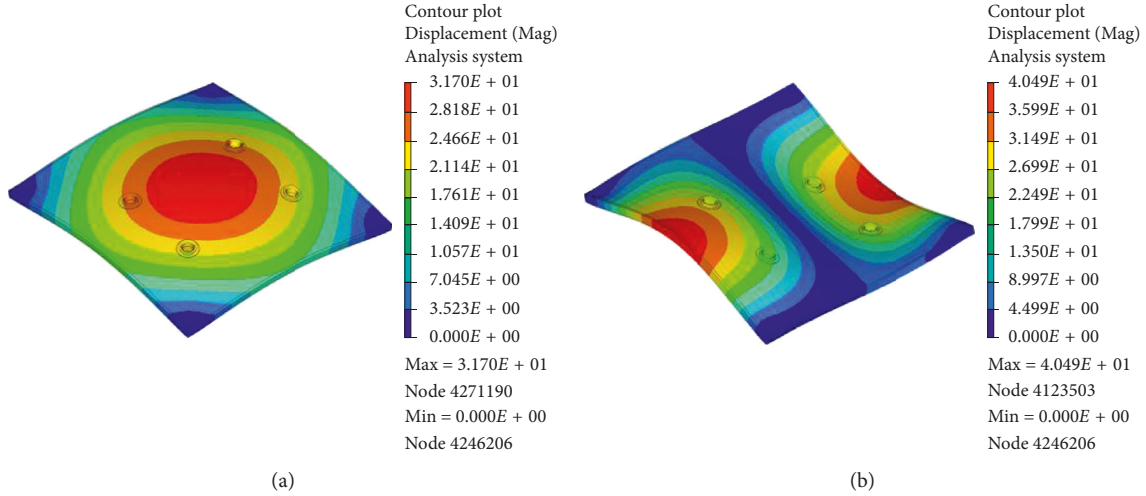


FIGURE 3: Simulation analysis of the mode shape. (a) First mode shape. (b) Second mode shape.

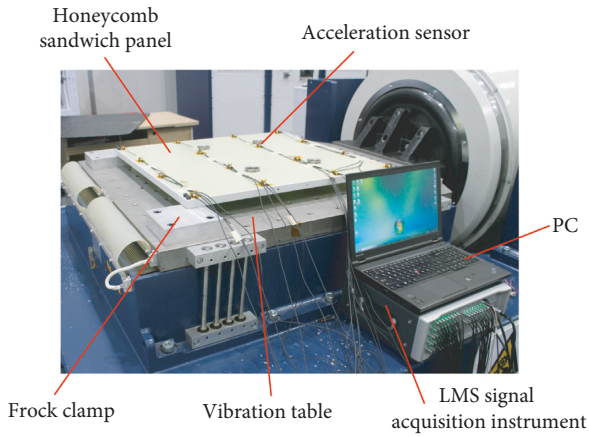


FIGURE 4: Modal test setup of satellite sailboard.

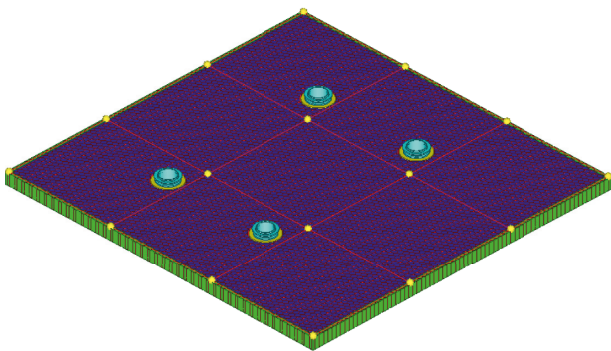


FIGURE 5: Sensor placement in the test.

The PSO algorithm simulates the migration and social behaviour in the foraging process of birds. First, a system initialises a group of random particles. Then, it continuously adjusts their flight direction and speed through their memory and the exchange of group information. Finally, the group reaches the optimal position.

The algorithm assumes that a particle swarm is composed of  $N$  particles, each of which has a  $d$ -dimensional

search space. The mathematical expressions of the particle's velocity and position at time are given by

$$\begin{aligned} v_{id}(t+1) &= v_{id}(t) + c_1 \xi (P_{id}(t) - x_{id}(t)) \\ &\quad + c_2 \zeta (P_{gd}(t) - x_{id}(t)), \\ x_{id}(t+1) &= x_{id}(t) + v_{id}(t+1). \end{aligned} \quad (3)$$

Here,  $i = 1, 2, \dots, N$  is the number of particles,  $d = 1, 2, \dots, D$  is the particle search dimension,  $v_i(t)$  and  $x_i(t)$  are the velocity and position of the  $i$ -th particle at time  $t$ ,  $P_i$  is the historical best position of the  $i$ -th particle search,  $P_g$  is the optimal position of the entire population,  $c_1$  and  $c_2$  are particle acceleration coefficients, and  $\xi$  and  $\zeta$  are random numbers that are uniformly distributed from 0 to 1. The above equations are for the basic PSO algorithm, whose particle flight principle is shown in Figure 9.

The flow of the PSO algorithm is shown in Figure 10.

**3.2. Sensitivity Analysis.** Errors are unavoidable in engineering calculations and tests. Error sources include the following factors:

- (1) *Stiffness Error.* This is the error caused by factors such as the thickness of a sheet, the modulus of elasticity of a material, and the stiffness of a joint between parts.
- (2) *Quality Error.* This is the error caused by factors such as structural feature simplification, material density, and auxiliary quality such as screws.
- (3) *Systematic Error.* This is the error caused by theoretical assumptions, structural discrepancies, iterative algorithms, signal acquisition, and the postprocessing of results during simulation and testing.

A sensitivity analysis method can be used to find a set of design parameters that are sensitive to a target. Let the design parameter of the initial finite element model be  $P$  and eigenvector  $\lambda$  be its implicit function. When parameter  $p$  changes slightly, the first-order Taylor expansion of the  $r$ -th feature quantity  $\{\lambda^{(r)}\}$  is given by [27]



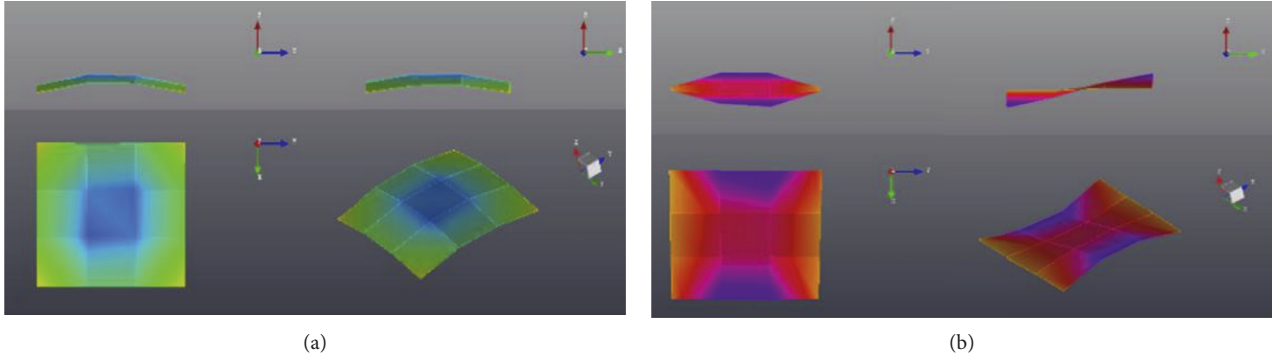


FIGURE 6: Mode shapes of the test. (a) First mode shape. (b) Second mode shape.

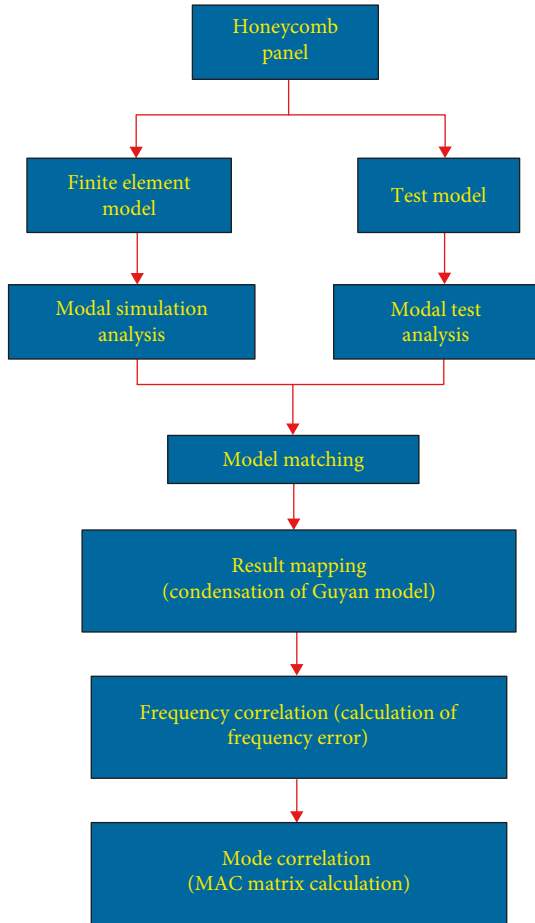


FIGURE 7: Block diagram of the correlation test.

$$\{\lambda^{(r)}(p + \Delta p)\} = \{\lambda^{(r)}(p)\} + \sum_{i=1}^n \frac{\partial \{\lambda^{(r)}\}}{\partial (p_r)} \Delta p_i. \quad (4)$$

The sensitivity matrix is expressed as [28]

$$S_\lambda = \begin{bmatrix} \frac{\partial \lambda_1}{\partial p_1} & \frac{\partial \lambda_1}{\partial p_2} & \cdots & \frac{\partial \lambda_1}{\partial p_n} \\ \vdots & \vdots & \ddots & \vdots \\ \frac{\partial \lambda_m}{\partial p_1} & \frac{\partial \lambda_m}{\partial p_2} & \cdots & \frac{\partial \lambda_m}{\partial p_n} \end{bmatrix}. \quad (5)$$

TABLE 2: Calculation results of model correlation.

| Modal order | Modal frequency |                 |           | MAC value |
|-------------|-----------------|-----------------|-----------|-----------|
|             | Test (Hz)       | Simulation (Hz) | Error (%) |           |
| 1           | 81.04           | 86.35           | -6.15     | 0.9287    |
| 2           | 141.5           | 154.7           | -8.53     | 0.8485    |
| 3           | 176.4           | 190.1           | -7.21     | 0.7528    |
| 4           | 207.2           | 227.9           | -9.08     | 0.6416    |
| 5           | 307.9           | 337.9           | -8.88     | 0.2901    |
| 6           | 350.3           | 392.4           | -10.73    | 0.0430    |
| 7           | 391.4           | 445.0           | -12.04    | 0.6965    |

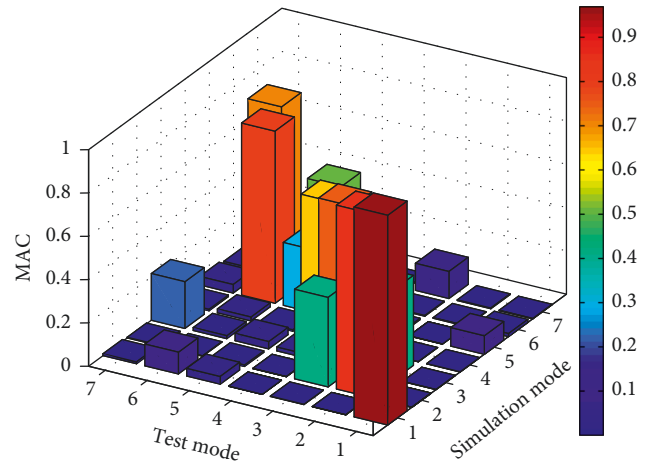


FIGURE 8: MAC value matching of simulation mode and test mode.

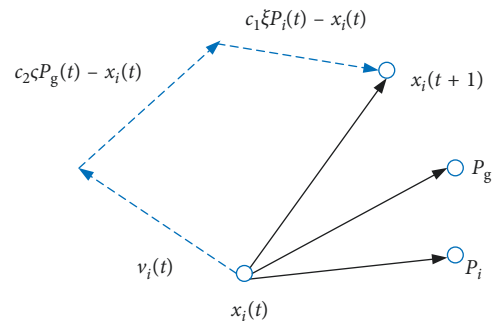


FIGURE 9: Principle of particle flight.

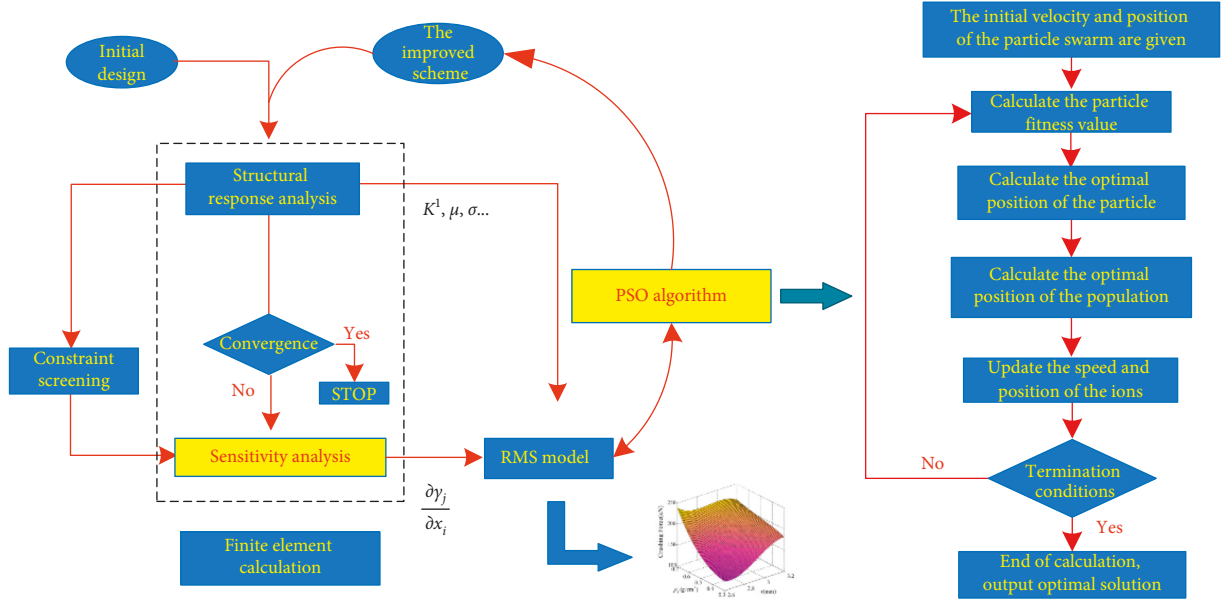


FIGURE 10: Operational logic diagram of the combined optimization algorithm.

In the above formula,  $n$  refers to the number of design parameters to be corrected,  $m$  is the number of feature quantities considered,  $\Delta\lambda$  is the residual vector, and  $\Delta p$  is the amount of change in the design parameter.

Therefore, the sensitivity matrix of the MAC value of the vibration correlation coefficient can be expressed as

$$S_{MAC} = \begin{bmatrix} \frac{\partial MAC_1}{\partial p_1} & \frac{\partial MAC_1}{\partial p_2} & \cdots & \frac{\partial MAC_1}{\partial p_n} \\ \vdots & \vdots & \ddots & \vdots \\ \frac{\partial MAC_m}{\partial p_1} & \frac{\partial MAC_m}{\partial p_2} & \cdots & \frac{\partial MAC_m}{\partial p_n} \end{bmatrix}. \quad (6)$$

Considering the structural vibrations of  $n$  degrees of freedom, the eigenvalue equation is given by

$$([K] - \lambda_r [M])\{\phi^{(r)}\} = \{0\}, \quad (7)$$

where  $[K]$  and  $[M]$  are the real-symmetric structural stiffness matrix and mass matrix of order  $n \times n$ , respectively,  $\lambda_r$  is the characteristic quantity of the  $r$ -th order of the structure, and  $\{\phi^{(r)}\}$  is the  $r$ -th order mode shape of the structure.

The formula of eigenvalue frequency sensitivity obtained using the orthogonality condition is given by

$$\frac{\partial\{\lambda^{(r)}\}}{\partial p_i} = \{\phi^{(r)}\}^T \left( \frac{\partial[K]}{\partial p_i} - \lambda_r \frac{\partial[M]}{\partial p_i} \right) \{\phi^{(r)}\}. \quad (8)$$

The sensitivity matrix of the mode shape correlation coefficient is expressed as

$$MAC_{ij} = \frac{(\{\phi_i^e\}^T \{\phi_j^a\})^2}{(\{\phi_i^e\}^T \{\phi_i^e\})(\{\phi_j^a\}^T \{\phi_j^a\})}, \quad (9)$$

where  $\phi_i^e$  is the  $i$ -th order test mode of vibration,  $\phi_j^a$  is the calculated  $j$ -th order mode of vibration obtained by the through finite element analysis, and superscript T indicates matrix transposition.

The sensitivity calculation formula of the mode shape correlation coefficient of the  $i$ -th modified design parameter,  $p_i$ , is as follows:

$$\frac{\partial MAC_{ij}}{\partial p_i} = \frac{2\{\phi_i^e\}^T \{\phi_j^a\} (\partial\{\phi_j^a\}/\partial p_i)}{(\{\phi_i^e\}^T \{\phi_i^e\})(\{\phi_j^a\}^T \{\phi_j^a\})} - \frac{2(\{\phi_i^e\}^T \{\phi_j^a\})^2 \{\phi_j^a\}^T (\partial\{\phi_j^a\}/\partial p_i)}{(\{\phi_i^e\}^T \{\phi_i^e\})(\{\phi_j^a\}^T \{\phi_j^a\})^2}, \quad (10)$$

where  $\partial\{\phi_j^a\}/\partial p_i$  is the partial derivative of the mode shape obtained by the  $j$ -th order finite element analysis model with respect to design parameter  $p_i$ .

The sensitivity analysis of the variables in Table 3 is carried out by considering the modal frequency for the first 7 orders and the correlation MAC value of the finite element model as response targets. As the order of magnitude varies significantly between variables, sensitivity also varies by different orders of magnitude, which is normalised for convenience in comparison [29, 30].

As seen in Figures 11(a) and 11(b), the modulus, density, and thickness of the panel, the modulus and density of the honeycomb, and the modulus of the frame are sensitive variables. Hence, they can be selected as model updating parameters for optimization.

**3.3. Model Updating.** Model updating is achieved by adjusting the stiffness and mass distribution of the finite

TABLE 3: Initial values of the elastic parameters and dimensions of the model.

| Attribute category    | Component name         | Corresponding number | Initial value |
|-----------------------|------------------------|----------------------|---------------|
| Elastic modulus (MPa) | Upper and lower panels | 1                    | 1.4E4         |
|                       | Frame                  | 2                    | 4.5E4         |
|                       | Compression sleeve     | 3                    | 1.2E5         |
|                       | Support base           | 4                    | 1.0E5         |
|                       | Honeycomb core         | 5                    | 7.2E4         |
| Density ( $T/mm^3$ )  | Upper and lower panels | 6                    | 1.85E-9       |
|                       | Frame                  | 7                    | 1.7E-9        |
|                       | Compression sleeve     | 8                    | 4.7E-9        |
|                       | Support base           | 9                    | 1.8E-9        |
|                       | Honeycomb core         | 10                   | 2.8E-9        |
| Thickness (mm)        | Upper and lower panels | 11                   | 2             |
|                       | Frame                  | 12                   | 0.5           |
|                       | Honeycomb core         | 13                   | 0.02          |

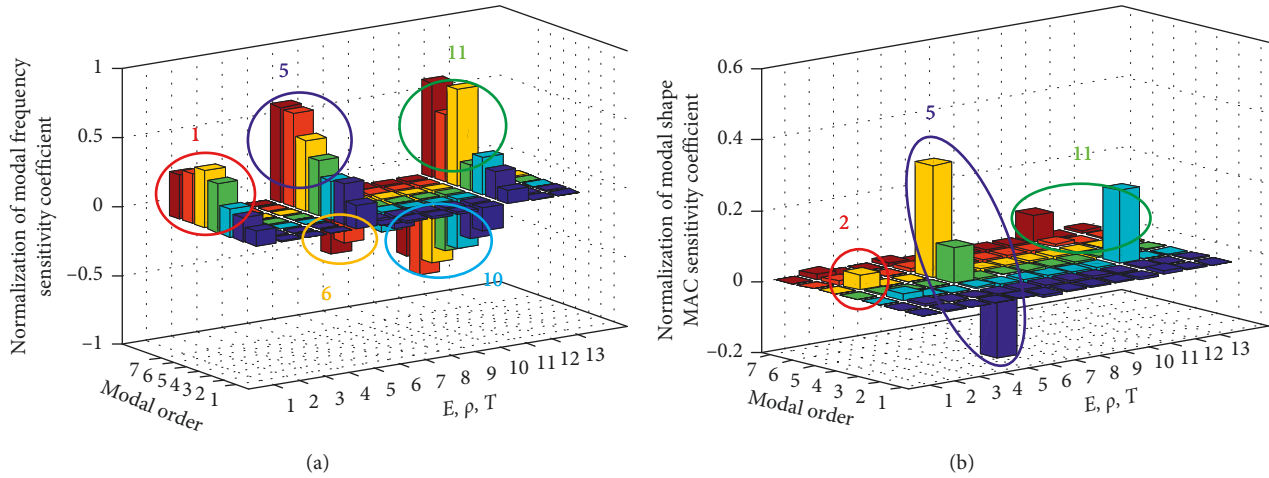


FIGURE 11: Sensitivity of the design parameters. (a) Sensitivity of modal frequency to design variables. (b) Sensitivity of modal shape MAC values to design variables.

element model [31]. The combined PSO + NLPQL iterative optimization strategy is used to find the final model parameter vector, and an error function is minimized with the least amount of model parameter modification to perform model updating [32]. The design variables are the six parameter variables determined after sensitivity analysis. The constraint condition is that the total mass of the model must not be more than 110%. The objective function has the smallest error function, that is, the error in the simulation and test frequency is close to zero, and the correlation MAC value is close to one.

The optimal model updating parameters and the comparison of the parameters before and after the updating are shown in Table 4.

The frequency and mode shape convergence of the modified model are shown in Figure 12.

The modified finite element model is obtained after optimization. The modal analysis is repeated to obtain a new natural frequency and mode shape, which are compared with the experimental values and simulation

result before the updating. The corrected results are provided in Table 5.

The corrected MAC matrix and the comparison of the frequency mode shapes for the first 7 orders are shown in Figures 13 and 14, respectively.

After optimization, the orthogonality of the simulated mode shape and the experimental mode shape is good. The low-order frequency error in the simulation model is less than 5%, the high-order error is less than 10%, and the modal confidence MAC is above 0.8. The modal frequency and mode shape of the optimized model are closer to the frequency and mode shape of the experimental mode. The model can more accurately reflect structural dynamic characteristics.

## 4. Model Updating Verification

**4.1. Frequency Response Test Verification.** Vibration response analysis is performed based on the modified finite element model to further verify the accuracy of the modified

TABLE 4: Comparison of initial and optimized values of model elastic parameters and dimensions.

| Number | Design variables                              | Initial value | Optimization value |
|--------|---|---------------|--------------------|
| 1      | Elastic modulus of panels (MPa)               | 1.4E4         | 1.52E4             |
| 2      | Elastic modulus of frame (MPa)                | 4.5E4         | 4.77E4             |
| 5      | Elastic modulus of honeycomb core (MPa)       | 7.2E4         | 6.91E4             |
| 6      | Density of panels ( $\text{mm}^3$ )           | 1.85E-9       | 1.74E-9            |
| 10     | Density of honeycomb core ( $\text{T/mm}^3$ ) | 2.8E-9        | 2.69E-9            |
| 11     | Thickness of panels (mm)                      | 2             | 2.02               |

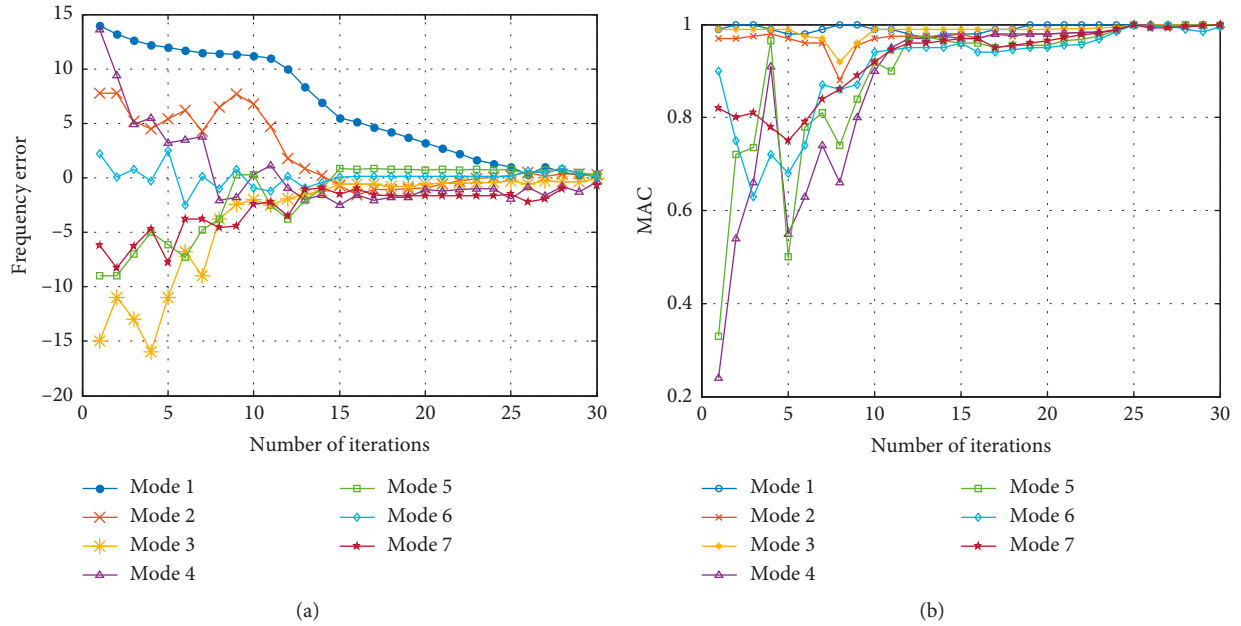


FIGURE 12: Modal convergence of the model during the updating process. (a) Convergence of frequency error during the updating process. (b) Convergence of MAC values during the updating process.

TABLE 5: Frequency error and MAC value of the model before and after updating.

| Modal order | Error before updating    |           | Error after updating     |           |
|-------------|--------------------------|-----------|--------------------------|-----------|
|             | Frequency $\epsilon$ (%) | MAC value | Frequency $\epsilon$ (%) | MAC value |
| 1           | -6.15                    | 0.9287    | -0.27                    | 0.9755    |
| 2           | -8.53                    | 0.8485    | -0.05                    | 0.9522    |
| 3           | -7.21                    | 0.7528    | -0.66                    | 0.9343    |
| 4           | -9.08                    | 0.6416    | -4.20                    | 0.9016    |
| 5           | -8.88                    | 0.2901    | -2.25                    | 0.8832    |
| 6           | -10.73                   | 0.0430    | -5.13                    | 0.8525    |
| 7           | -12.04                   | 0.6965    | -8.79                    | 0.8241    |

model. The test conditions for sine sweep are provided in Table 6.

The geometrical centroid position of the honeycomb panel is selected as the reference point, and the simulation and experimental acceleration responses of sine sweep and random vibration are compared. The frequency response test setup and measurement point arrangement are shown in Figure 15.

The simulation and test results of the sine sweep resonance frequency and its response value are compared in

each direction. The comparison results are shown in Table 7.

The Z direction of the satellite sailboard (perpendicular to the plane of the board) is a key consideration for the sailboard under working conditions, and it is the most typical in a complex space environment. Four measurement points are arranged on the surface of the sailboard, i.e., at the fixed position of the sailboard, the middle of the sailboard close to the long side, the centre of the plane of the sailboard structure, and in the vicinity of a fire connection device.



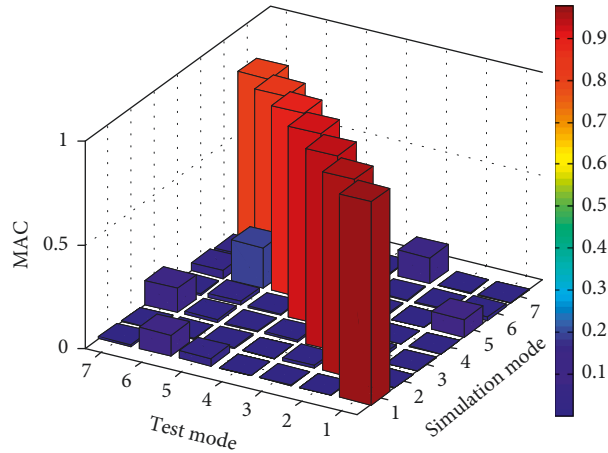


FIGURE 13: Updated MAC matrix.

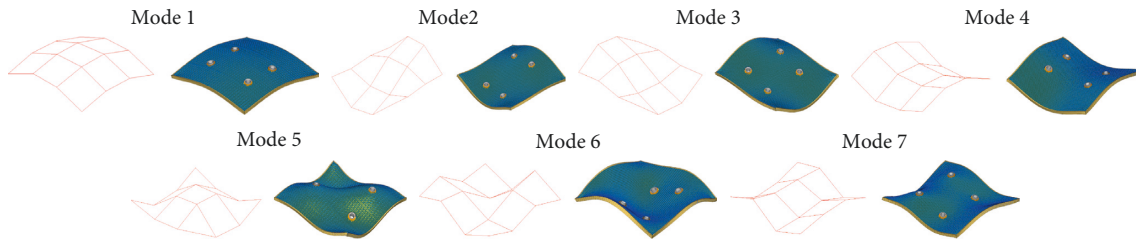


FIGURE 14: Comparison of the modified 7th order simulation mode and test mode shapes for the first 7 orders.

TABLE 6: Sine sweep loading conditions.

| Frequency range (Hz) | Amplitude |
|----------------------|-----------|
| 5–8                  | 2.48 mm   |
| 8–65                 | 2 g       |
| 65–100               | 4 g       |
| Loading direction    | X, Y, Z   |

Simulation and experimental values are obtained at the four points, as shown in Figure 16.

4.2. *Random Test Verification.* Uncertain mechanical vibrations must be simulated and analysed to meet space launch requirements. The loading condition of the structure is determined by the response result. Based on the comprehensive specific working conditions of aerospace, only the acceleration response within 2000 Hz is considered to simplify the research object while ensuring research significance. Table 8 shows the conditions of random vibration excitation.

The simulation and experimental root mean square values of random vibration acceleration are compared in all directions and the results are shown in Table 9.

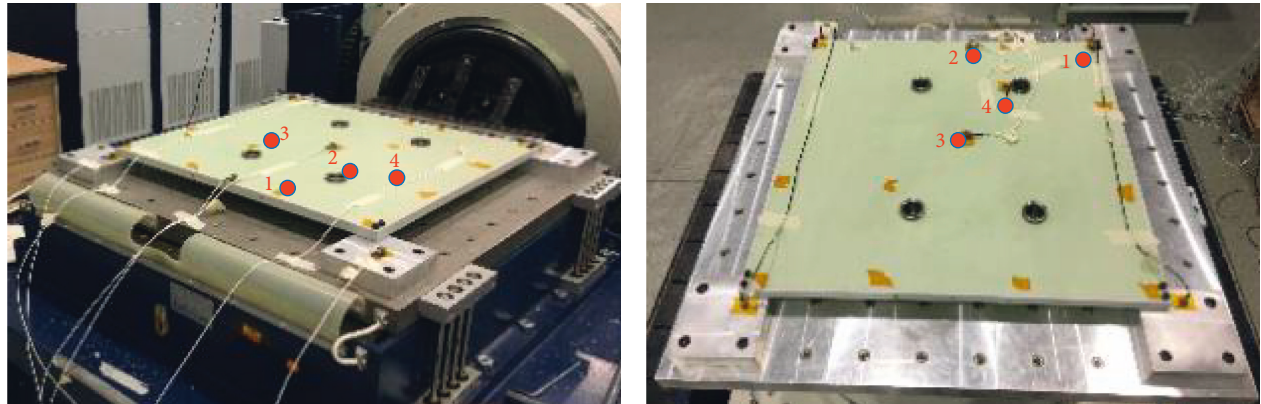
The simulation and experimental random vibration response curves of the satellite sailboard at the centre measurement point in the Z direction (perpendicular to the plane of the board) are shown in Figures 17(a) and 17(b), respectively.

The figure shows that the acceleration response curves at the reference point obtained through the test and simulation are consistent and that amplitude and frequency errors are within an acceptable range.

## 5. Conclusion

Structural sensitivity analysis (SOL200) is performed based on a finite element model developed using NAS-TRAN. The model updating method can significantly improve the precision of the finite element model, which is of considerable engineering and practical significance. During the design, the objective function and constraint conditions can be determined according to the specific requirements of structural performance. By selecting appropriate design variables through sensitivity analysis, satisfactory structures can be obtained through optimization.

Compared with the single gradient method and intelligent optimization algorithm, the combined optimization strategy exhibits higher reliability and better universality. This can provide balance between optimization efficiency and optimization quality and ensure the global optimization of a solution as much as possible. The RMS method is used to establish an approximate model of structural response in the implementation of the combined optimization strategy, which can replace the actual finite element calculation model and considerably reduce the number of structural heavy analysis.



(a)

(b)

FIGURE 15: Frequency response test setup. (a) Measurement point arrangement in X and Y directions. (b) Measurement point arrangement in Z direction.

TABLE 7: Comparison of sine sweep resonance frequency and its response value.

| Axis | Simulation    |                | Test          |                | Error     |           |
|------|---------------|----------------|---------------|----------------|-----------|-----------|
|      | Amplitude (g) | Frequency (Hz) | Amplitude (g) | Frequency (Hz) | Amplitude | Frequency |
| X    | 2.26          | 141.2          | 2.14          | 135.3          | 5.61%     | 4.36%     |
| Y    | 2.35          | 176.5          | 2.27          | 171.6          | 3.52%     | 2.86%     |
| Z    | 10.06         | 80.02          | 10.35         | 81.46          | -2.80%    | -1.77%    |

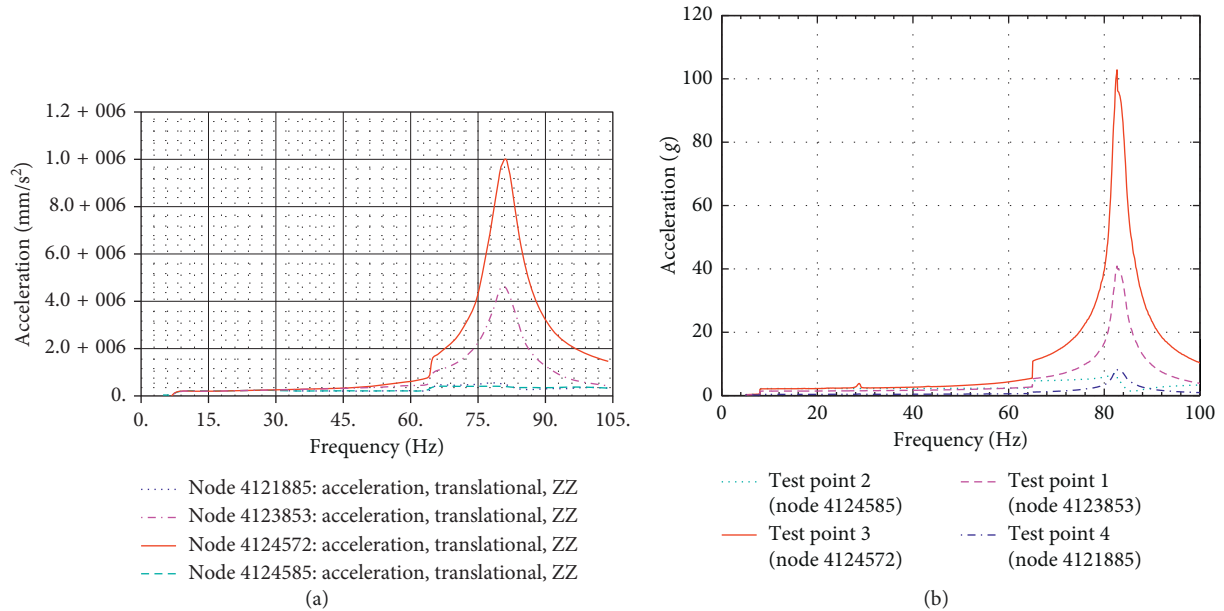


FIGURE 16: Frequency response curves at reference points in the Z direction. (a) Simulation curves. (b) Experimental curves.

TABLE 8: Loading conditions for random vibration excitation.

| Frequency range (Hz)                       | Power spectral density |
|--|------------------------|
| 20–100                                     | 3 dB/oct               |
| 100–600                                    | 0.1 g <sup>2</sup> /Hz |
| 600–2000                                   | -9 dB/oct              |
| Total root mean square value ( $G_{RMS}$ ) | 9.648                  |
| Loading direction                          | X, Y, Z                |
| Time                                       | 1 min per direction    |

TABLE 9: Comparison of sinusoidal sine sweep resonance frequency and its response value.

| Direction | Simulation                 | Test                       | Error                |
|-----------|----------------------------|----------------------------|----------------------|
|           | Acceleration ( $g_{RMS}$ ) | Acceleration ( $g_{RMS}$ ) | Root mean square (%) |
| X         | 30.44                      | 28.91                      | 5.29                 |
| Y         | 37.25                      | 35.49                      | 4.96                 |
| Z         | 45.06                      | 46.78                      | -3.68                |

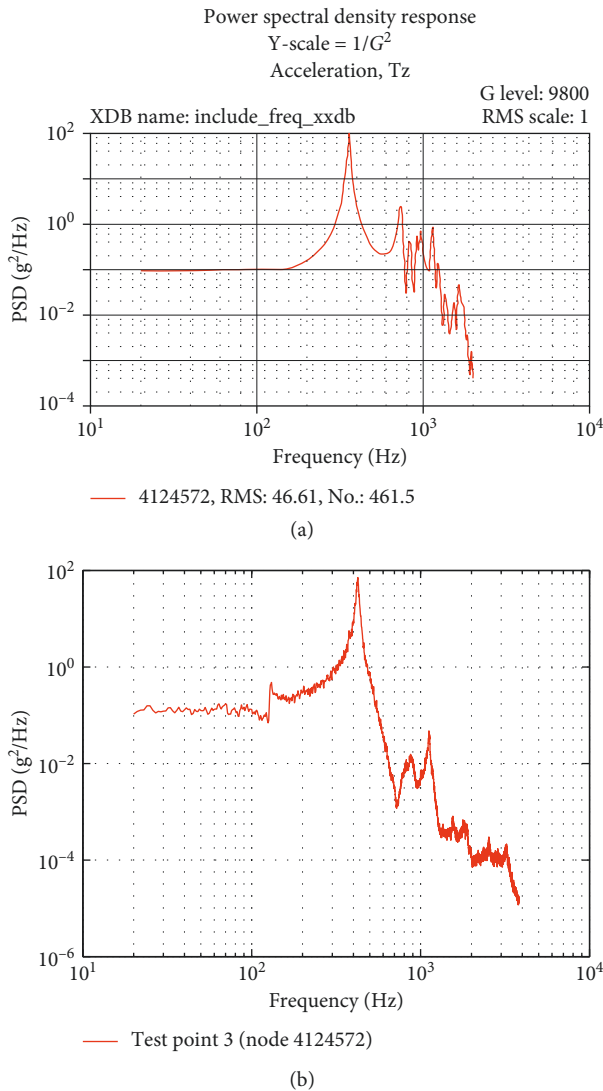


FIGURE 17: Random vibration response curves at reference point 3 in the Z direction. (a) Simulation curve. (b) Experimental curve.

Based on the proposed model updating method, the finite element model of a certain satellite panel structure is modified using the modal test data and excitation response data of a vibration table. It is verified that the simulation accuracy of the model is significantly improved.

### Data Availability

The data used in this study may be made available upon request to the authors.

### Conflicts of Interest

The authors declare that there are no conflicts of interest regarding the publication of this paper.

### Acknowledgments

This research was financially supported by the National Natural Science Foundation of China (51505470) and Youth

Innovation Promotion Association, CAS (2018237), and Jiang Xin-song Innovation Fund (20180504).

### References

- [1] T. Mukhopadhyay and S. Adhikari, "Equivalent in-plane elastic properties of irregular honeycombs: an analytical approach," *International Journal of Solids & Structures*, vol. 91, pp. 169–184, 2016.
- [2] L. Boldrin, S. Hummel, F. Scarpa et al., "Dynamic behaviour of auxetic gradient composite hexagonal honeycombs," *Composite Structures*, vol. 149, pp. 114–124, 2016.
- [3] Y. Tanimoto, T. Nishiwaki, T. Shiomi, and Z. Maekawa, "A numerical modeling for eigenvibration analysis of honeycomb sandwich panels," *Composite Interfaces*, vol. 8, no. 6, pp. 393–402, 2011.
- [4] M. A. Yahaya, D. Ruan, G. Lu, and M. S. Dargusch, "Response of aluminium honeycomb sandwich panels subjected to foam projectile impact—an experimental study," *International Journal of Impact Engineering*, vol. 75, pp. 100–109, 2015.
- [5] P. Liu, Y. Liu, and X. Zhang, "Internal-structure-model based simulation research of shielding properties of honeycomb sandwich panel subjected to high-velocity impact," *International Journal of Impact Engineering*, vol. 77, pp. 120–133, 2015.
- [6] M. Rebillat and X. Boutillon, "Identification of honeycomb sandwich properties by high-resolution modal analysis," in *Proceedings of the International Conference on Experimental Mechanics*, vol. 6, no. 14, p. 1221, EPJ Web of Conferences, France, December 2010.
- [7] L. T. Wang, L. Y. Hua, Y. F. Wang et al., "Structural modal analysis of electric satellite with metallic honeycomb board," in *Proceedings of the 2017 5th International Conference on Mechanics and Mechatronics*, Tokyo, Japan, June 2018.
- [8] H. Rahman, R. Jamshed, H. Hameed, and S. Raza, "Finite element analysis (FEA) of honeycomb sandwich panel for continuum properties evaluation and core height influence on the dynamic behavior," *Key Engineering Research*, vol. 326, pp. 1–10, 2011.
- [9] G. Steenackers, J. Peeters, B. Ribbens, and C. Vuye, "Development of an equivalent composite honeycomb model: a finite element study," *Applied Composite Materials*, vol. 23, no. 6, pp. 1177–1194, 2016.
- [10] M. K. Khan, K. Bashir, S. Moizuddin, and S. Hussain, "Natural frequency determination and modal analysis of prototype structure of honeycomb sandwich panels," in *Proceeding of the International Conference on Recent Advances in Space Technologies IEEE*, pp. 193–199, Istanbul, Turkey, June 2007.
- [11] H. Luo, G. Liu, S. Ma et al., "Dynamic analysis of the spacecraft structure on orbit made up of honeycomb sandwich plates," in *Proceedings of the International Conference on Computer Science and Automation Engineering IEEE*, pp. 83–87, Shanghai, China, June 2011.
- [12] K. Zheng, W. H. Liao, and Y. T. Qin, "Analysis and research of honeycomb sandwich structure for micro-satellite based on equivalent theory," *Key Engineering Materials*, vol. 426–427, pp. 472–476, 2010.
- [13] Z. Bai, Y. Zhao, W. Ma, and H. Tian, "Modal analysis for small satellite system with finite element method," in *Proceedings of the International Symposium on Systems and Control in Aerospace and Astronautics IEEE*, pp. 1–5, Shenzhen, China, December 2008.

- [14] L. Guj and A. Sestieri, "Dynamic modeling of honeycomb sandwich panel," *Archive of Applied Mechanics*, vol. 77, no. 11, pp. 779–793, 2007.
- [15] S. Debruyne, D. Vandepitte, and D. Moens, "Identification of design parameter variability of honeycomb sandwich beams from a study of limited available experimental dynamic structural response data," *Computers & Structures*, vol. 146, pp. 197–213, 2015.
- [16] S. Vempati and T. Mahender, "Modal analysis of honeycomb sandwich panel," *International Journal of Research in Engineering & Advanced Technology*, vol. 4, no. 5, pp. 14–17, 2016.
- [17] A. Abbadi, Y. Koutsawa, A. Carmasol, S. Belouettar, and Z. Azari, "Experimental and numerical characterization of honeycomb sandwich composite panels," *Simulation Modelling Practice & Theory*, vol. 17, no. 10, pp. 1533–1547, 2009.
- [18] S. D. Papka and S. Kyriakides, "Experiments and full-scale numerical simulations of in-plane crushing of a honeycomb," *Acta Materialia*, vol. 46, no. 8, pp. 2765–2776, 1998.
- [19] X. E. Guo and L. J. Gibson, "Behavior of intact and damaged honeycombs: a finite element study," *International Journal of Mechanical Sciences*, vol. 41, no. 1, pp. 85–105, 1999.
- [20] D. Ruan, G. Lu, B. Wang, and T. X. Yu, "In-plane dynamic crushing of honeycombs a finite element study," *International Journal of Impact Engineering*, vol. 28, no. 2, pp. 161–182, 2002.
- [21] Z. Zou, S. R. Reid, P. J. Tan, S. Li, and J. J. Harrigan, "Dynamic crushing of honeycombs and features of shock fronts," *International Journal of Impact Engineering*, vol. 36, no. 1, pp. 165–176, 2009.
- [22] Z. Zheng, J. Yu, and J. Li, "Dynamic crushing of 2D cellular structures: a finite element study," *International Journal of Impact Engineering*, vol. 32, no. 1–4, pp. 650–664, 2005.
- [23] D. Dan, Y. Chen, and B. Xu, "A PSO driven intelligent model updating and parameter identification scheme for cable-damper system," *Shock and Vibration*, vol. 2015, Article ID 423898, 14 pages, 2015.
- [24] N. Hu, P. Zhou, and J. Yang, "Comparison and combination of NLPQL and MOGA algorithms for a marine medium-speed diesel engine optimization," *Energy Conversion & Management*, vol. 133, pp. 138–152, 2017.
- [25] A. Navid, S. Khalilarya, and H. Taghavifar, "Comparing multi-objective non-evolutionary NLPQL and evolutionary genetic algorithm optimization of a DI diesel engine: DoE estimation and creating surrogate model," *Energy Conversion & Management*, vol. 126, pp. 385–399, 2016.
- [26] J. Fu, H. Luo, M. Yu, and G. Liu, "Finite element model updating based on sensitivity analysis for 5-DOF manipulator," in *Proceedings of the Information Technology and Mechatronics Engineering Conference IEEE*, pp. 1187–1192, Chongqing, China, October 2017.
- [27] R. Huñady, "A sensitivity analysis of the dynamic behavior of aluminium honeycomb sandwich panels," *American Journal of Mechanical Engineering*, vol. 4, no. 7, pp. 236–240, 2016.
- [28] P. G. Bakir, E. Reynders, and G. D. Roeck, "Sensitivity-based finite element model updating using constrained optimization with a trust region algorithm," *Journal of Sound and Vibration*, vol. 305, no. 1-2, pp. 211–225, 2007.
- [29] M. Sanayei, A. Khaloo, M. Gul, and F. Necati Catbas, "Automated finite element model updating of a scale bridge model using measured static and modal test data," *Engineering Structures*, vol. 102, pp. 66–79, 2015.
- [30] A. Mirzaee, R. Abbasnia, and M. Shayanfar, "A comparative study on sensitivity-based damage detection methods in bridges," *Shock & Vibration*, vol. 4, pp. 1–19, 2015.
- [31] W. G. Zhang and Y. Liu, "Main factor sensitivity analysis based on response surface model updating of port crane structure," *Journal of Coastal Research*, vol. 73, pp. 166–172, 2015.
- [32] P. Vanhonacker, "Differential and difference sensitivities of natural frequencies and mode shapes of mechanical structures," *Aiaa Journal*, vol. 18, no. 12, pp. 1511–1514, 2015.



